Investigation of copper oxidation states in plasmonic nanomaterials by XAS and Raman spectroscopy

Clemence Queffelec, Florian Forato, Bruno Bujoli, D. Andrew Andrew Knight, Emiliano Fonda, Bernard Humbert

Journal Name

ARTICLE

Investigation of copper oxidation states in plasmonic nanomaterials by XAS and Raman spectroscopy

Received 00th January 20xx,
Accepted 00th January 20xx

DOI: 10.1039/x0xx00000x

Clémence Queffélec,*[a] Florian Forato,[a] Bruno Bujoli,[a] D. Andrew Knight,[b] Emiliano Fonda,[c] and Bernard Humbert*[d]

Plasmonic core-shell-isolated nanoparticles are promising nanoplatforms for photocatalysis and for low detection analysis. This paper describes the characterization of a 2,2'-bipyridine phosphonate functionalized Ag@TiO_2 nanocomposite wich complexes copper ions by enhanced Raman spectroscopy and X-ray absorption (XANES and EXAFS). We distinguished Cu(I) from Cu(II) complexes using shell-isolated nanoparticle enhanced Raman (SHINERS) combined with XAS spectroscopy.

Introduction

Ag@TiO_2 core-shell nanoparticles in which a Cu(I)/bipyridine (bpy) complex was grafted onto the oxide shell surface was recently shown to be an active catalyst in the Ullmann reaction under blue laser irradiation.[1] We now wish to establish the mechanism of the reaction and correlate the catalytic mechanism and plasmonic effects (e.g. thermal, "hot electron" or redox).[2–7] The mechanism of the Ullmann reaction is a subject of much debate, and different mechanisms have been proposed in the literature, depending on whether the catalysis is heterogeneous or homogeneous, and whether assisted by light.[8–15] The most commonly described mechanisms for this reaction are a classical catalytic oxidation pathway and reductive elimination, or a radical pathway. So we assume that under plasmonic excitation, if the classical catalytic oxidation mechanism is occurring, the oxidation of copper will change, most likely from copper(I) to copper(II). In that regard, we decided to combine X-ray absorption near edge structure spectroscopy (XANES) that will give information on the oxidation state of copper and Raman spectroscopy that will provide information on the ligand's coordination to the metal ion.[16,17] It is very difficult to predict how copper will be coordinated, or its oxidation state during the catalytic cycle, and these have not been described for organic/inorganic hybrid plasmonic nanomaterials.

Recently, in our nanoassemblies, surface enhanced Raman spectroscopy (SERS) measurements showed that an enhanced electrical field was localized near the surface of the core-shell metallic NPs interface under irradiation, in the region of the silver plasmon resonance.[18] To distinguish the different copper species involved in the catalytic cycle, it is essential to be able to probe the oxidation state of copper ions and their molecular environment simultaneously. This paper demonstrates the possibility of coupling SERS and XAS spectroscopies for the characterization of nanohybrid catalysts. XAS spectroscopy is a relevant technique for studying the structure of metal complexes because X-ray absorption near-edge structure (XANES) will give information on the oxidation state of the metal and extended X-Ray absorption fine structure (EXAFS) will provide information on copper's local environment. This technique has been used frequently to describe copper(II) complexes[17,19–23] but fewer examples of organic copper(I)/complexes have been reported.[24] SERS is a well-established technique used for rapid monitoring of molecular and ionic species evolution.[25–31] However, the assignment of SERS signals can be subject to interpretation. Therefore, coupling XANES and SERS to characterize representative species involved in catalysis is essential before monitoring in situ the photocatalytic reactions. Herein, we report the first studies on copper/bpy complexes on plasmonic active support where the active state of copper was compared between commercially available and synthesized copper samples by XANES. The neighboring bpy ligand was studied by Raman spectroscopy and EXAFS.

[a] Université de Nantes, CNRS, CEISAM, UMR 6230, F-44000 Nantes, France. E-mail : clemence.queffelec@univ-nantes.fr
[b] Department of Biomedical & Chemical Engineering & Sciences, Florida Institute of Technology, 150 West University Boulevard, Melbourne, Florida, 32901, USA
[c] Synchrotron SOLEIL, L'ormes des merisiers, Saint Aubin BP-48, 91192, Gif-Sur-Yvette Cedex, France
[d] Institut des Matériaux Jean Rouxel, CNRS-Université de Nantes, 2 rue de la Houssinière, B.P. 32229, 44322 Nantes Cedex 3, France. E-mail : Bernard.Humbert@cnrs-imn.fr

Electronic Supplementary Information (ESI) available: [Common structure of copper(I) and copper(II) complexes references, Normalized absorbance vs E spectrum for copper(I) and copper(II) samples, EXAFS fitting of Ag@TiO_2@bpy-PA-Cu(II) and Cu(I) complexes, photos of home-made cell used for Raman spectroscopy, Comparison of Raman spectrum]. See DOI: 10.1039/x0xx00000x

Materials and methods

Starting materials.

All reagent chemicals and solvents were purchased from commercial sources (Aldrich, Acros, SDS) and used as received. The syntheses of the ligand bpy-PA and Ag@TiO_2@bpy-PA-Cu NPs have been reported previously.[1,18]

Nanoparticle characterization.

Nanoparticle morphology was investigated by transmission electron microscopy (TEM, 1230 Jeol) working at a voltage of 120 keV, using holey carbon-coated copper grids (300 mesh) to gain sufficient electronic contrast.

Raman spectroscopy.

Raman spectra were recorded using a microconfocal Raman inVia™ Reflex Renishaw device. The instrument was equipped with a double edge filter to eliminate the Rayleigh scattering, and a charged couple device (CCD) camera working at a temperature of 220 K and with a 1024 by 256 pixel array. Laser excitations used were 457.9, 488, 514.53, 632.82 and 785 nm wavelengths. The setup was composed of a confocal microscope that was equipped with an automated XYZ table. The spectral resolution achieved with the use of gratings of 2400, 1800 or 1200 grooves per millimetre was between 2 and 3.5 cm^{-1} according to the excitation wavelength. All the Raman characteristics (optical responses vs wavelength, vs polarisation, wavenumber accuracy, stability etc.) were calibrated based on previous methods. The accuracy of the wavenumber, verified with the silicon Raman signal, was better than 0.5 cm^{-1}. The focused power of the laser beam was also checked for each wavelength to avoid any transformation or heating of the samples. Accordingly, the power was kept below 100 μW/μm2 and the magnitudes×50 and x20 of the objective (numerical aperture respectively of 0.75 and 0.35 and then a spot size of around respectively of 1.5 and 15 μm^2) has been selected after a test list. The confocal mode was also sometimes used to select a smaller analyzed volume in the same irradiated volume and to record Raman spectra with the better lateral spatial resolution (around at λ/2) in order to check the heterogeneity of our films. The acquisition time was between 1 s and 30 s in order to obtain an enough signal-to noise ratio without damaging the samples.

For sample preparation, colloidal solutions of Ag@TiO_2@bpy-PA-Cu(II) were dropped onto silica slides under a flow of argon gas until water evaporation, approximately fifteen successive evaporations are needed in order to obtain a suitable amount.

For copper(I) samples, the aqueous colloidal solution of Ag@TiO_2@bpy-PA was centrifuged, water was removed and the NPs were rinsed with HPLC grade acetonitrile several times. The colloidal solution was then transferred into a glove box, degassed for 15 min. A solution of $[Cu(ACN)_4]PF_6$ (ACN = acetonitrile) in degassed acetonitrile (10 mM) was then added to the colloidal solution and the resulting solution was stirred for 5 h. Then, the solution was dropped several times onto a silica slide and when dried, the slide was transferred into a home-made cell that were kept under argon.

XANES spectroscopy.

Cu K-edge XANES data were collected on the SAMBA beamline at Soleil synchrotron (Saint-Aubin, France). The energy calibration was made versus a copper foil standard setting the maximum of the first derivative at 8979 eV. The copper references were measured in transmission mode. XANES spectra of Ag@TiO_2@bpy-Cu samples were collected in fluorescence mode. Spectra were normalized using Horae software package.[32]

For sample preparation, the colloidal solution Ag@TiO_2@L-Cu(II) was mixed with boron nitride, and the mixture was dried and a pellet was formed. The XANES spectrum was recorded directly on the pellet. For Ag@TiO_2@L-Cu(I), because copper(I) oxidized really fast into copper(II), the sample was handled in a glove bag under Argon, was mixed with boron nitride, and the mixture was dried and a pellet was formed. Then, the sample has been kept under an helium bag under the laser beam to be able to record XANES overnight.

EXAFS data analysis

The χ(k) data were Fourier transformed (FT) in the k range between 3 and 11 $Å^{-1}$ for Ag@TiO_2@bpy-Cu(II) and 3 to 9 $Å^{-1}$ for Ag@TiO_2@bpy-Cu(I). The range for fitting in r-space was from 1 to 3.3 Å for both compounds. The amplitudes and phases for the scattering paths for coordination models were calculated using Feff 6. The amplitude reduction factor (S_0^2) was found to be 0.92±0.02by fitting the first shell of a copper foil. Multiple scattering was taken into account to model the bpy ligand contribution to the EXAFS signal.

Data were fitted in r-space using theoretical standards obtained on a similar structure including two bpy ligands and nitrate in the coordination shell around copper. The structure has been simplified in order to fit data with a reduced number of parameters: bpy was represented by the coordinating nitrogen and by two types of carbon atoms at approximately (C1) 2.85 and (C2) 3.05 Å. The number of carbon atoms was constrained to match those of nitrogen in the first shell, one bpy coordinated meaning 2N+2C1+2C2. Then additional oxygen atoms were included in the simulation when it turned out to be necessary, the criterion guiding the insertion of new parameters being a reduction of reduced chi square. It has been necessary to include two type of multiple scattering paths connected with bpy: Cu-N-C1-Cu and Cu-N-C2-Cu that did not required in first approximation additional free parameters. We used an average Debye Waller factor for the first coordination shell and a second one for the multiple scattering, C1 and C2. In the case of Cu(II) we have been leaded to include two O atoms, O1 and O2, while in the case of Cu(I) only one was identified. Table S1 in the supporting information reports all used structural parameters.

Results and discussion

1. Synthesis and TEM characterization of nanomaterials

Plasmonic copper(II) and copper(I) nanomaterials were synthesized as described previously.[1,18] TEM images of the system Ag@TiO_2@bpy-PA-Cu(II) is presented in Figure 1 and for

Ag@TiO_2@bpy-PA-Cu(I) in Figure S1. The nanomaterials synthesized are silver spherical nanoparticles with an average diameter around 20 nm in a TiO_2 matrix.

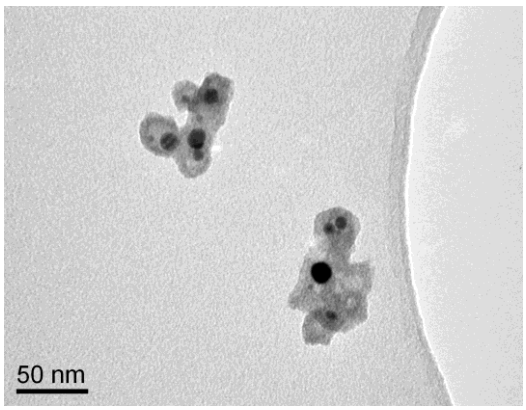

Figure 1. TEM image of Ag@TiO_2@bpy-PA-Cu(II)

2. XAS measurements

The preparation of samples for XAS studies is described in the supporting information. First, the oxidation state of metal was determined by comparison of the absorption edge position of the Cu K-edge for four samples, two commercially available salts $[Cu(I)(ACN)_4]PF_6^-$ and $Cu(II)(NO_3)_2 \bullet 2.5H_2O$) and two prepared compounds $Cu(I)(phen)_2PF_6$ and $Cu(II)(bpy)_2(NO_3)_2$ (ACN = acetonitrile, bpy = 2,2'-bipyridine, phen = 1,10-phenanthroline). Their general coordination is shown in Figure S1. It is known that the Cu K-edge absorption edge will slightly shift towards higher energy values when the oxidation state of the metal increases. Also, in organic complexes, the Cu K-edge, compared with the absorption spectrum of inorganic compounds, is shifted slightly towards higher energy values.[33,34] Figure 2 shows the XANES spectra for reference materials.

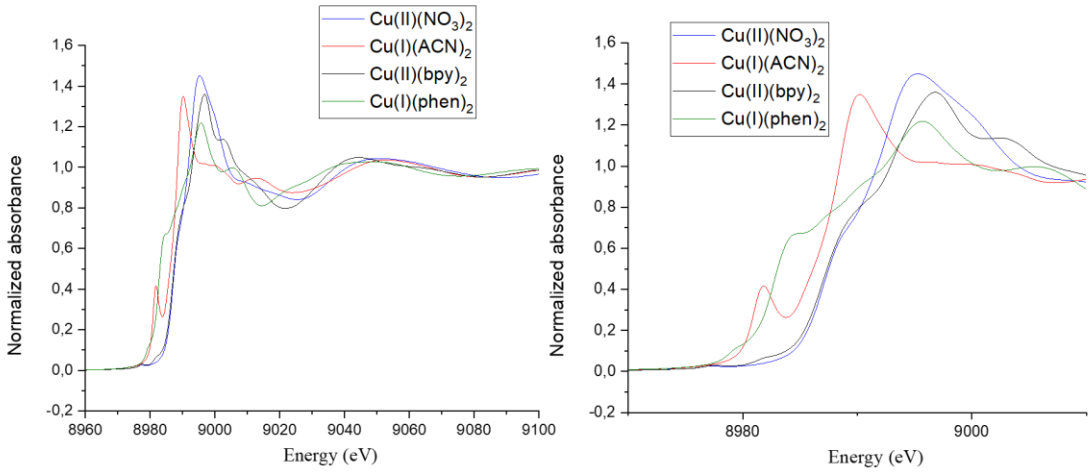

Figure 2. Normalized absorbance vs E spectrum for the four reference complexes. Red: $Cu(ACN)_4PF_6^-$, blue : $Cu(NO_3)_2 \bullet 2.5H_2O$, green: $Cu(I)(phen)_2$, black : $Cu(II)(bpy)_2$. On the right, zoom of the 8975-9100 eV.

The figure clearly shows the difference in the shape and features of the edge as well as the chemical shifts. In copper(I) containing samples, the peak at the rising part of the edge at 8982 eV is quite predominant compared to copper(II) where the peak is almost non-visible. This pre-edge feature in copper(I) is attributed to the 1s → 4p transition[24,33] and Kau et al. showed that the intensity of this transition is related to the coordination geometry of copper.[33] In $Cu(ACN)_4PF_6^-$, the pre-edge absorption is very intense and in this complex, copper atoms are in a nearly local ideal tetrahedral symmetry. For the $Cu(I)(phen)_2$ complex, the pre-edge is weakest and a shoulder can be observed at 8985 eV. The Cu(I) complex geometry is distorted[35] towards the Cu(II) complex preferred geometry which is either a square planar or an octahedral geometry with an inversion center.[20,21] For copper(II) samples, the profiles are quite similar; only in $Cu(II)(bpy)_2$, the shoulder observed in $Cu(I)(phen)_2$ is present but much weaker. Gaur et al.[21] demonstrated that at 8985 eV the edge feature could be assigned to copper(II) square pyramidal complexes. Then, the two plasmonically active copper containing Ag@TiO_2 samples were investigated by XANES. Figure 3 shows the XANES spectra of Ag@TiO_2@bpy-PA-Cu(II) and Ag@TiO_2@bpy-PA-Cu(I). The figure clearly shows again the difference in the shape and features at the edge absorption as well as an edge absorption drift. In the copper(I) sample, the peak in the rising part of the edge is quite predominant compared to copper(II) and is located at 8981 eV. This allows us to suggest that the local symmetry of our complex might be closer to the $Cu(ACN)_4PF_6^-$ geometry (Figure S2) and that the 1s to 4p transition is present. Two, three or four coordinate copper(I) complexes possess pre-edge peaks ranging from 8980 to 8985 eV.[36] In comparison, the copper(II) structure within the plasmonic material is similar to both reference complexes confirming +2 oxidation state (Figure S3). This first observation indicates that we clearly distinguish the +1

oxidation state from the +2 oxidation state of Cu ions in the plasmonic material.

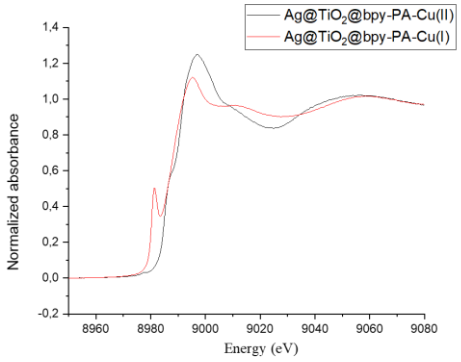

Figure 3: Normalized absorbance vs E spectrum for two plasmonic nanomaterial. Red: Ag@TiO_2@L-Cu(I), Black: Ag@TiO_2@L-Cu(II)

To provide evidence for coordination geometry around copper ions and to get the different structural parameters for the nearest neighbouring shell, EXAFS has been recorded. The fitting of the experimental data to the theoretical model is described in the supporting information and Table 1 shows the local structure parameters concerning nearest neighbors for both nanomaterials.

Table 1. EXAFS parameters. N = number of atoms, R = nearest neighbour distance and σ^2 = Debye-Waller. The error in the last digit is reported in parentheses.

Material	N	R (Å)	σ^2 (10^{-3}Å^2)
Ag@TiO_2@bpy-PA-Cu(I)	2	1.90(1)	3(1)
	1	2.04(2)	
Ag@TiO_2@bpy-PA-Cu(II)	4	1.96(1)	5(2)
	1	2.44(4)	
	1	2.60(5)	

The data fitting for both Ag@TiO_2@bpy-PA-Cu(II) and Ag@TiO_2@bpy-PA-Cu(I) is shown in Figure 4 as well as original data quality and EXAFS fitting in Figure S4.

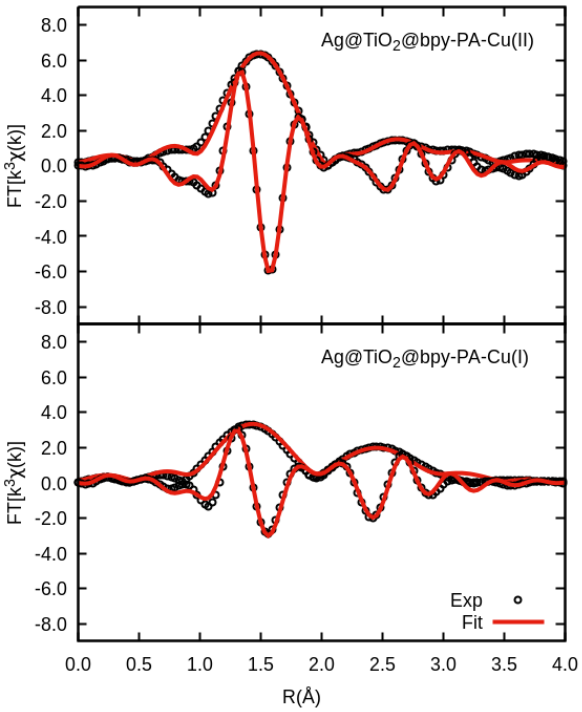

Figure 4. Fourier transforms of k3 weighted EXAFS signals (dots) and simulations (red lines) of Cu(II) containing composites (top) and Cu(I) containing ones (bottom). Same bounds have been used to compare Fourier transforms.

On the basis of EXAFS analyses, we tentatively suggest that in its first coordination sphere Cu(II) possesses approximatively four bonded nitrogen atoms with bond length of 1.96(1)Å and two more atoms of similar Z (most likely oxygen given the possible coordinating ligands) at a long distance of 2.44(4)Å and 2.60(5) Å comparable to those of oxygen of water coordinated to Cu(II) in pseudo octahedral complexes as [Cu(bpdc)(en)(H_2O)$_2$] reported by Pirsiavash et al..[37]
Cu(I) possesses a more complex structure with a more asymmetric environment in the first coordination sphere. Our best model includes one bpy ligand with two nitrogen atoms at 1.90(1) Å and an elongated distance to a second light atom (i.e. C, N or O) at 2.04(2) Å, which is consistent with a low-coordinate copper(I) geometry.[39,40,38] The reduced coordination of Cu(I) versus Cu(II) is accompanied by a marked reduction of all coordination distances. Our final EXAFS simulations were based on the hypothesis that one or two bpy were coordinating Cu, these are the simulated curves shown in Figures 4 and S4, thus we can provide additional information concerning next nearest neighbours (nearest C atoms of bpy) in Table S1.

In addition, to probe the local environment of copper, i.e. the organic component of the complex, we performed Raman spectroscopy. The preparation and set-up used in those experiments are described in the Supporting Information and Figure S5. SERS were recorded on both copper(I) and copper(II) systems. We have already demonstrated that on Ag@TiO_2@bpy-PA, prior to coordination with copper, the best feature was obtained at 633 nm, with a low power laser, and the spectrum displayed different modes of bipyridine.[18] Then, we compared spectra of Ag@TiO_2@bpy-PA, Ag@TiO_2@bpy-PA-Cu(II) and Ag@TiO_2@bpy-PA-Cu(I) (Figure 5). The signal at 290 cm^{-1} observed for Ag@TiO_2@bpy-PA-Cu(I) is assigned to the vibrational modes of a Cu-N bond on the basis of experimental XANES data. Similarly the Cu(II)-N vibrational mode is observed around 230 cm^{-1} as demonstrated in our previous paper.[18] In addition, different peaks could be observed and were attributed to different modes of vibration of bipyridine. A small shift in the wavenumber values for the bipyridine modes could be observed after copper complexation, confirming that copper is coordinated to the bipyridine skeleton (Figure S6). Also, vibrational modes of bipyridine are characterized by the difference in Raman activity due probably to different coordination and geometry around the copper ions (inset in Figure 5). This is again in agreement with the near-edge peak observed in XANES spectra and EXAFS fitting. Finally, the peak related to Ag-N around 250-260 cm^{-1} was not present in the sample confirming again that copper is coordinated to the nitrogen atoms of bipyridine.

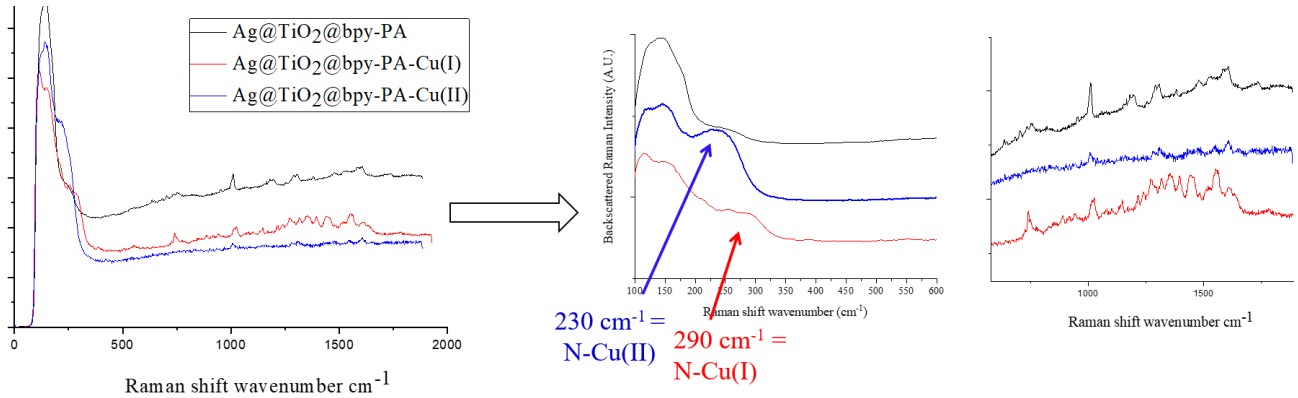

Figure 5. Comparison of Raman spectra of Ag@TiO_2@bpy-PA, Ag@TiO_2@bpy-PA-Cu(II) and Ag@TiO_2@bpy-PA-Cu(I) at 633 nm (power density: 75 µWµm² for Ag@TiO_2@bpy-PA and Ag@TiO_2@bpy-PA-Cu(II) and 15 µWµm² for Ag@TiO_2@bpy-PA-Cu(I)).

Finally, the apparent broadening of the signals between 200 and 300 cm^{-1} might be due to (i) the experimental data are presented without any numerical treatment and we have not subtracted the background signal (ii) the low wavenumber signals are enhanced by the near field of the plasmonic structure and some local heating effects might be involved as well.

Conclusion

In conclusion, we have demonstrated that with the help of XANES and EXAFS features and Raman spectroscopy, we were able to probe and characterize copper(I) or copper(II) complexes on plasmonic core-shell nanomaterials. These results provide significant information that was proven valuable for determining both the oxidation state and ligand complex geometry for copper. For future work we will record in situ XANES spectra for a specific catalytic reaction in order to monitor the oxidation state of copper under laser irradiation, and simultaneously record RAMAN spectra to monitor the ligand-complex structural evolution. This should help to unravel the mechanism occurring during laser assisted photocatalysis.

Conflicts of interest

There are no conflicts to declare.

Acknowledgements

The authors acknowledge financial support from the “Centre National de la Recherche Scientifique” (CNRS) through the PICS COSMOCAT. They would like to thank Soleil Synchrotron for beam time provided under project number 20180025 and G. Alizon for technical assistance during the experiment.

References

1 F. Forato, S. Talebzadeh, B. Bujoli, C. Queffelec, S. A. Trammell and D. A. Knight, Core-Shell Ag@TiO_2 Nanocomposites for Low-Power Blue Laser Enhanced Copper(I) Catalyzed Ullmann Coupling, *Chemistryselect*, 2017, **2**, 769–773.

2 J. Szczerbinski, L. Gyr, J. Kaeslin and R. Zenobi, Plasmon-Driven Photocatalysis Leads to Products Known from E-beam and X-ray-Induced Surface Chemistry, *Nano Lett.*, 2018, **18**, 6740–6749.

3 S. M. Kim, S. W. Lee, S. Y. Moon and J. Y. Park, The effect of hot electrons and surface plasmons on heterogeneous catalysis, *J. Phys.-Condens. Matter*, 2016, **28**, 254002.

4 H. Zhang, T. Itoi, T. Konishi and Y. Izumi, Dual Photocatalytic Roles of Light: Charge Separation at the Band Gap and Heat via Localized Surface Plasmon Resonance To Convert CO_2 into CO over Silver-Zirconium Oxide, *J. Am. Chem. Soc.*, 2019, **141**, 6292–6301.

5 H. Huang, L. Zhang, Z. Lv, R. Long, C. Zhang, Y. Ling, K. Wei, C. Wang, L. Chen, Z.-Y. Li, Q. Zhang, Y. Luo and Y. Xiong, Unraveling Surface Plasmon Decay in Core-Shell Nanostructures toward Broadband Light-Driven Catalytic Organic Synthesis, *J. Am. Chem. Soc.*, 2016, **138**, 6822–6828.

6 X. Sun, Y. Zou and J. Jiang, Surface plasmon resonances enhanced click chemistry through synergistic photothermal and hot electron effects, *Chem. Commun.*, 2019, **55**, 4813–4816.

7 X. Zhang, X. Li, M. E. Reish, D. Zhang, N. Q. Su, Y. Gutierrez, F. Moreno, W. Yang, H. O. Everitt and J. Liu, Plasmon-Enhanced Catalysis: Distinguishing Thermal and Nonthermal Effects, *Nano Lett.*, 2018, **18**, 1714–1723.

8 E. Sperotto, G. P. M. van Klink, G. van Koten and J. G. de Vries, The mechanism of the modified Ullmann reaction, *Dalton Trans.*, 2010, **39**, 10338–10351.

9 C. J. Judd, S. L. Haddow, N. R. Champness and A. Saywell, Ullmann Coupling Reactions on Ag(111) and Ag(110); Substrate Influence on the Formation of Covalently Coupled Products and Intermediate Metal-Organic Structures, *Sci. Rep.*, 2017, **7**, 14541.

10 H. Goksu, Y. Yildiz, B. Celik, M. Yazici, B. Kilbas and F. Sen, Highly Efficient and Monodisperse Graphene Oxide Furnished Ru/Pd Nanoparticles for the Dehalogenation of Aryl Halides via Ammonia Borane, *Chemistryselect*, 2016, **1**, 953–958.

11 A. Basagni, L. Ferrighi, M. Cattelan, L. Nicolas, K. Handrup, L. Vaghi, A. Papagni, F. Sedona, C. Di Valentin, S. Agnoli and M. Sambi, On-surface photo-dissociation of C-Br bonds: towards room temperature Ullmann coupling, *Chem. Commun.*, 2015, **51**, 12593–12596.

12 R. N. Dhital, C. Kamonsatikul, E. Somsook and H. Sakurai, Bimetallic gold-palladium alloy nanoclusters: an effective catalyst for Ullmann coupling of chloropyridines under ambient conditions, *Catal. Sci. Technol.*, 2013, **3**, 3030–3035.

13 S. E. Creutz, K. J. Lotito, G. C. Fu and J. C. Peters, Photoinduced Ullmann C-N Coupling: Demonstrating the Viability of a Radical Pathway, *Science*, 2012, **338**, 647–651.

14 M. Majek and A. Jacobi von Wangelin, Ambient-Light-Mediated Copper-Catalyzed C-C and C-N Bond Formation, *Angew. Chem.-Int. Ed.*, 2013, **52**, 5919–5921.

15 N. Marina, A. E. Lanterna and J. C. Scaiano, Expanding the Color Space in the Two-Color Heterogeneous Photocatalysis of Ullmann C-C Coupling Reactions, *Acs Catal.*, 2018, **8**, 7593–7597.

16 Y. Deng, A. D. Handoko, Y. Du, S. Xi and B. S. Yeo, In Situ Raman Spectroscopy of Copper and Copper Oxide Surfaces during Electrochemical Oxygen Evolution Reaction: Identification of CuIII Oxides as Catalytically Active Species, *ACS Catal.*, 2016, **6**, 2473–2481.

17 A. Patlolla, P. Baumann, W. Xu, S. D. Senanayake, J. A. Rodriguez and A. I. Frenkel, Characterization of Metal-Oxide Catalysts in Operando Conditions by Combining X-ray Absorption and Raman Spectroscopies in the Same Experiment, *Top. Catal.*, 2013, **56**, 896–904.

18 F. Forato, S. Talebzadeh, N. Rousseau, J.-Y. Mevellec, B. Bujoli, D. A. Knight, C. Queffelec and B. Humbert, Functionalized core-shell Ag@TiO_2 nanoparticles for enhanced Raman spectroscopy: a sensitive detection method for Cu(ii) ions, *Phys. Chem. Chem. Phys.*, 2019, **21**, 3066–3072.

19 A. Gaur, B. D. Shrivastava, D. C. Gaur, J. Prasad, K. Srivastava, S. N. Jha, D. Bhattacharyya, A. Poswal and S. K. Deb, EXAFS study of binuclear hydroxo-bridged copper(II) complexes, *J. Coord. Chem.*, 2011, **64**, 1265–1275.

20 A. Wolska, M. T. Klepka, W. Ferenc and A. Drzewiecka-Antonik, XAFS studies of Cu(II) and Co(II) complexes with derivatives of cinnamic acid, *X-Ray Spectrom.*, 2015, **44**, 323–329.

21 A. Gaur, W. Klysubun, N. N. Nair, B. D. Shrivastava, J. Prasad and K. Srivastava, XAFS study of copper(II) complexes with square planar and square pyramidal coordination geometries, *J. Mol. Struct.*, 2016, **1118**, 212–218.

22 M. Larsson, J. B. Linden, S. Kaur, B. Le Cerf and I. Kempson, Cu K-edge XANES: polymer, organic, inorganic spectra, and experimental considerations, *Powder Diffr.*, 2017, **32**, S28–S32.

23 A. Drzewiecka, A. E. Koziol, M. T. Klepka, A. Wolska, S. B. Jimenez-Pulido, T. Lis, K. Ostrowska and M. Struga, Two coordination modes around the Cu(II) cations in complexes with benzo[b]furancarboxylic acids, *Chem. Phys. Lett.*, 2013, **559**, 41–45.

24 B. E. Etschmann, J. R. Black, P. V. Grundler, S. Borg, D. Brewe, D. C. McPhail, L. Spiccia and J. Brugger, Copper(I) speciation in mixed thiosulfate-chloride and ammonia-chloride solutions: XAS and UV-Visible spectroscopic studies, *RSC Adv.*, 2011, **1**, 1554–1566.

25 S. Fateixa, H. I. S. Nogueira and T. Trindade, Hybrid nanostructures for SERS: materials development and chemical detection, *Phys. Chem. Chem. Phys.*, 2015, **17**, 21046–21071.

26 I. J. Jahn, O. Žukovskaja, X.-S. Zheng, K. Weber, T. W. Bocklitz, D. Cialla-May and J. Popp, Surface-enhanced Raman spectroscopy and microfluidic platforms: challenges, solutions and potential applications, *Analyst*, 2017, **142**, 1022–1047.

27 Y.-F. Huang, D.-Y. Wu, H.-P. Zhu, L.-B. Zhao, G.-K. Liu, B. Ren and Z.-Q. Tian, Surface-enhanced Raman spectroscopic study of p-aminothiophenol, *Phys. Chem. Chem. Phys.*, 2012, **14**, 8485–8497.

28 R. Panneerselvam, G.-K. Liu, Y.-H. Wang, J.-Y. Liu, S.-Y. Ding, J.-F. Li, D.-Y. Wu and Z.-Q. Tian, Surface-enhanced Raman spectroscopy: bottlenecks and future directions, *Chem. Commun.*, 2018, **54**, 10–25.

29 M. Moskovits, Persistent misconceptions regarding SERS, *Phys. Chem. Chem. Phys.*, 2013, **15**, 5301–5311.

30 N. Oyamada, H. Minamimoto, Y. Wakisaka and K. Murakoshi, Determination of Molecular Orientation in Bi-analyte Mono-molecule Layer through Electrochemical Surface-enhanced Raman Scattering Measurements, *Chem. Lett.*, 2019, **48**, 820–823.

31 K. Zhang, Y. Liu, Y. Wang, J. Zhao and B. Liu, Direct SERS tracking of a chemical reaction at a single 13 nm gold nanoparticle, *Chem. Sci.*, 2019, **10**, 1741–1745.

32 B. Ravel and M. Newville, ATHENA, ARTEMIS, HEPHAESTUS: data analysis for X-ray absorption spectroscopy using IFEFFIT, *J. Synchrotron Radiat.*, 2005, **12**, 537–541.

33 L. S. Kau, D. J. Spira-Solomon, J. E. Penner-Hahn, K. O. Hodgson and E. I. Solomon, X-ray absorption edge determination of the oxidation state and coordination number of copper. Application to the type 3 site in Rhus vernicifera laccase and its reaction with oxygen, *J. Am. Chem. Soc.*, 1987, **109**, 6433–6442.

34 W. E. Allen and T. N. Sorrell, Hydroxylation of an Aliphatic C–H Bond in an Imidazole-Ligated (μ-η2:η2-Peroxo)dicopper(II) Complex, *Inorg. Chem.*, 1997, **36**, 1732–1734.

35 S. Lopez and S. W. Keller, New Linear Coordination Polymers Based on Copper(I) and 4,7-Phenanthroline: Structure Dependence on Solvent and Counteranion, *Inorg. Chem.*, 1999, **38**, 1883–1888.
36 R. Sarangi, X-ray absorption near-edge spectroscopy in bioinorganic chemistry: Application to $M–O_2$ systems, *Coord. Chem. Rev.*, 2013, **257**, 459–472.
37 F. Pirsiavash, V. Amani and A. Abedi, Coordination number in copper(II) complexes with bipyridine-dicarboxylate anion and diamine derivatives, *Res. Chem. Intermed.*, 2018, **44**, 7411–7426.
38 R. K. GUPTA, M. YADAV, R. PANDEY and D. S. PANDEY, Synthesis and characterization of some heteroleptic copper(II) complexes based on meso-substituted dipyrrins, *J. Chem. Sci.*, 2011, **123**, 819–826.
39 K. B. Nilsson and I. Persson, The coordination chemistry of copper(I) in liquid ammonia, trialkyl and triphenyl phosphite, and tri-n-butylphosphine solution, *Dalton Trans.*, 2004, 1312–1319.
40 D. Kakizoe, M. Nishikawa, Y. Fujii and T. Tsubomura, Photophysical properties of three coordinated copper(I) complexes bearing 1,10-phenanthroline and a monodentate phosphine ligand, *Dalton Trans.*, 2017, **46**, 14804–14811.